Layered C 3 N 3 S 3 Polymer/Graphene Hybrids as Metal-Free Catalysts for Selective Photocatalytic Oxidation of Benzylic Alcohols under Visible Light

ARTICLE *in* ACS CATALYSIS · SEPTEMBER 2014

Impact Factor: 9.31 · DOI: 10.1021/cs5006597

7 AUTHORS, INCLUDING:

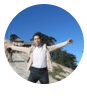

Zizhong Zhang
Fuzhou University
34 PUBLICATIONS **611** CITATIONS
SEE PROFILE

Huaxiang Lin
Fuzhou University
31 PUBLICATIONS **253** CITATIONS
SEE PROFILE

Xuxu Wang
Fuzhou University
215 PUBLICATIONS **3,761** CITATIONS
SEE PROFILE

Jinlin Long
Fuzhou University
64 PUBLICATIONS **1,064** CITATIONS
SEE PROFILE

ACS Catalysis

Letter

pubs.acs.org/acscatalysis

Layered $C_3N_3S_3$ Polymer/Graphene Hybrids as Metal-Free Catalysts for Selective Photocatalytic Oxidation of Benzylic Alcohols under Visible Light

Jie Xu, Liufeng Luo, Guangrui Xiao, Zizhong Zhang, Huaxiang Lin, Xuxu Wang, and Jinlin Long*

Institute Research of Photocatalysis, State Key Lab of Photocatalysis on Energy and Environment, College of Chemistry, Fuzhou University, Fuzhou 350116, P. R. China

Supporting Information

ABSTRACT: Metal-free carbon-based hybrids composed of reduced graphene oxide (rGO) and $C_3N_3S_3$ polymers with a layered "sandwich" structure were fabricated by an in situ two-step polymerization strategy and used as visible light photocatalysts for selective aerobic oxygenation of benzylic alcohols to the corresponding aldehydes, at good efficiency and high selectivity. This work shows the great potential and prospective application of the metal-free $C_3N_3S_3$ polymer in the photocatalyzed synthesis of fine chemicals.

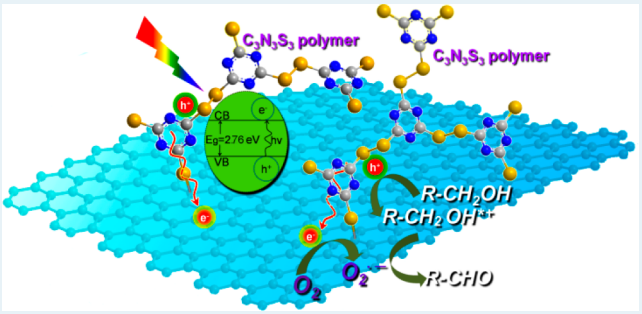

KEYWORDS: *$C_3N_3S_3$ polymer, graphene, hybrids, metal-free photocatalysis, selective oxidation*

The controlled and selective oxidation of alcohols to their corresponding aldehydes, ketones, or carboxylic acids is one of the most important reactions in organic chemistry and has always been a hot topic in both academic and industrial areas. The traditional methods to produce such fine chemicals involve commonly the use of noble metal catalysts including Pt, Pd, Au, among others, or organic oxidants such as 2, 2, 6, 6-tetramethylpiperidine oxide (TEMPO).[1−7] However, enormous disadvantages, such as toxicity, corrosiveness, expensive cost, poisoning, and deactivation,[8] greatly restricted the further improvement of the chemical processes. Photocatalysis, a booming green technology, affords a promising alternative to transform organic compounds into fine chemicals because it is low in cost and environmentally benign,[9] and as a result, it is receiving more and more attention.[1] Much effort has been devoted to the broad research from inorganic metal oxides, metal sulfides, mono-, and multiple-component composites for photofunctional materials capable of performing an excellent conversion and selectivity to the "green" synthesis of fine chemicals.[10−18] However, only few works have applied metal-free photocatalysts for the organic conversions. For example, Su et al. reported that mesoporous carbon nitride (mpg-C_3N_4) can effectively catalyze the selective oxidation of different aromatic alcohols under visible-light irradiation.[15]

Herein, we reported another example of the photocatalysis-driven organic transformations with a metal-free photocatalyst based on a $C_3N_3S_3$ polymer with delocalized π bonds. Our previous work showed that the $C_3N_3S_3$ polymer could function as a photocatalyst for hydrogen production under visible light irradiation.[19] A further exploration was performed to evaluate the photocatalytic oxidation capability of the pure $C_3N_3S_3$ polymer by using the selective photocatalytic oxidation of benzylic alcohol as a model reaction. A conversion of 28% is achieved with visible light irradiation of 8 h, indicating a promising application of the polymer in green organic transformation.

For improving the photocatalytic efficiency, graphene, which has been widely considered as one of the next-generation nanofillers for polymer nanocomposites,[20−25] was used as the framework and support for the $C_3N_3S_3$ polymer to improve the separation and transport of the photogenerated electrons and holes.[13,26−30] A well-dispersed state of graphene can guarantee a maximal surface area. It affects the neighboring $C_3N_3S_3$ polymer chains and, consequently, the properties of the whole matrix.[31] Many works showed that a stable aqueous dispersion of graphene can be obtained by reducing chemically graphene oxide (GO) with hydrazine hydrate and ammonia solution,[32,33] which results in reduced graphene oxide (rGO). The simple loading of the $C_3N_3S_3$ polymer on graphene is limited for the improvement of photocatalytic efficiency, even deleterious. In order to effectively hinder the restacking of graphene monolayer sheets during the reduction process, an innovative strategy is employed herein for preparation of the "sandwich" rGO/$C_3N_3S_3$ polymer hybrids as depicted in Scheme 1. A series of the layered rGO/$C_3N_3S_3$ hybrids with different rGO/$C_3N_3S_3$ polymer weight ratios (denoted as *x*rGO−CNS, where *x* is the rGO content) were fabricated by

Received: May 14, 2014
Revised: August 23, 2014

   dx.doi.org/10.1021/cs5006597 | ACS Catal. 2014, 4, 3302−3306

Scheme 1. Diagrammatic Sketch of Fabrication Procedures for the rGO/$C_3N_3S_3$ Hybrids

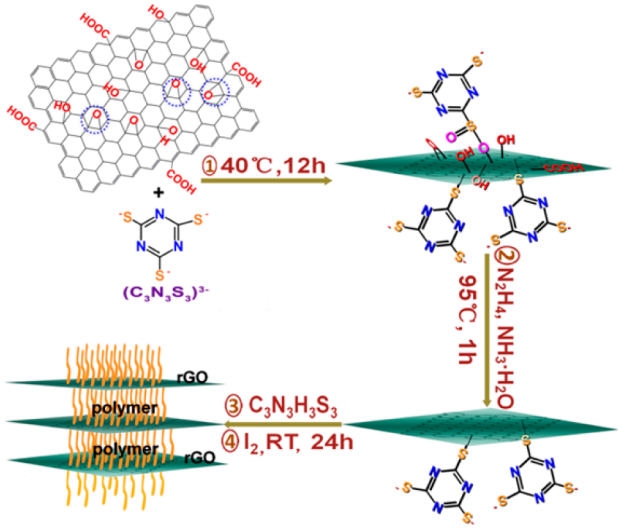

the in situ stepwise polymerization strategy to screen out an optimal photocatalyst.

The morphology and structure of the final products, rGO/$C_3N_3S_3$ polymer hybrids, were observed first by scanning electron microscope (SEM). The pure $C_3N_3S_3$ polymer particles accumulate in a random way (Figure 1A), whereas

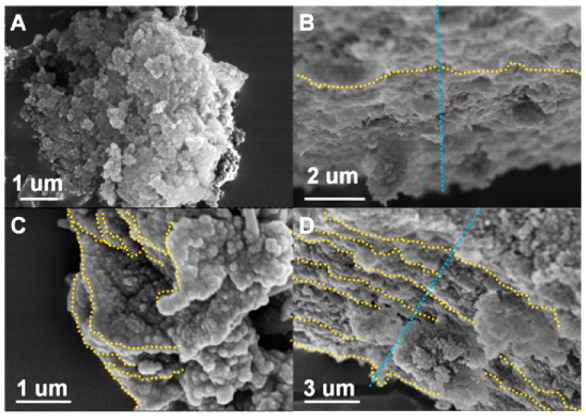

Figure 1. SEM images of pure $C_3N_3S_3$ polymer (A), 0.1rGO−CNS (B), 0.3rGO−CNS (C), and 2.0rGO−CNS (D).

the rGO/$C_3N_3S_3$ hybrids pack in a regular way (Figure 1B−D). The "sandwich"-like structure formed by the ordered stacking of rGO and $C_3N_3S_3$ polymer is clearly discernible for the three hybrids, 0.1rGO−CNS, 0.3rGO−CNS, and 2.0rGO−CNS. It is thus reasonable to believe that the intimate contact between the polymer and rGO can facilitate the transfer of photogenerated electrons from the $C_3N_3S_3$ polymer to the rGO moieties, consequently improving the photocatalytic efficiency.

The textural properties of the pure polymer and the rGO/$C_3N_3S_3$ hybrids with different graphene percentages were investigated by nitrogen adsorption−desorption at 77 K, as shown in Figure 2. All of the pure polymer and these hybrids display a type IV isotherm according to the IUPAC classification.[34] It appears that the pure polymer has a type H1 hysteresis among the four types of hysteresis loops, which is the characteristic of solids consisting of particles crossed by

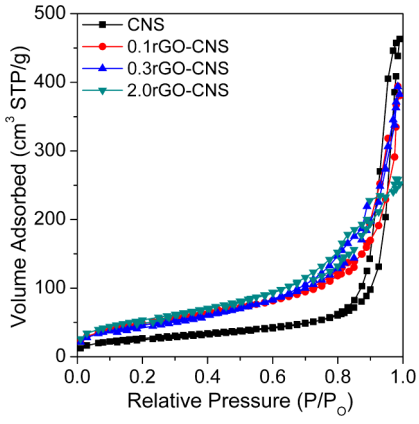

Figure 2. Nitrogen adsorption−desorption isotherms of pure CNS and *x*rGO−CNS samples.

nearly cylindrical channels or made by aggregates (consolidated) or agglomerates (unconsolidated), whereas the shape of the loops for these hybrids are much closer to the type H4, which is the characteristic of slit-shaped pores (plates or edged particles like cubes) usually found on solids consisting of particle aggregates or agglomerates.[33−35] The difference in porous properties originates from the insertion of rGO, corresponding to the SEM results. Moreover, the BET surface areas are doubled to 193 $m^2{\cdot}g^{-1}$ after the addition of 2.0 wt % rGO, compared to the pure polymer (94 $m^2{\cdot}g^{-1}$), which may result in a higher adsorption capacity and more possibility available to reactive substrates.

Fourier transform infrared spectroscopy (FTIR), a powerful technique for indentifying the structure of matter at the molecular scale, was used to monitor the formation of the rGO/$C_3N_3S_3$ hybrids. As shown in the Supporting Information, Figure S1a, a sharp and strong absorbance of 1125 cm^{-1} is observed for the $H_3C_3N_3S_3$ monomer, which represents the stretching vibration of >C═S. The peaks located at the range of 2900−3160 cm^{-1} belong to the stretching vibration of >N−H, and the peak at 1540 cm^{-1} is attributed to the combination of >N−H and C−N groups. These vibration bands are in accordance with the results reported by Loughran and Mieczys,[36,37] showing that the monomer exists in the form of ketone. Different from the monomer, the vibration bands at 2900−3160, 1360, and 1125 cm^{-1} disappear for the $C_3N_3S_3$ anchored on GO. Several peaks display at 1725, 1483, 1234, and 827 cm^{-1}, which correspond, respectively, to the stretching vibration of >C═N < , the six-membered ring of symmetrical triazines, and >N−C<, and the out-of-plane bending vibration of symmetrical triazines, indicating the appearance of polymerization. Moreover, the intense peak occurring at 966 cm^{-1} in the Raman spectra proves the existence of S−S bond (Supporting Information, Figure S2). The aforementioned analysis indicates that the grafted $C_3N_3S_3$ polymer exists in the form of trithiol. The identical IR and Raman (Supporting Information, Figure S2) spectra of the rGO/$C_3N_3S_3$ hybrids and the pure $C_3N_3S_3$ polymer indicate that the hybrids have the same chemical structure as the $C_3S_3N_3$ polymer.

XPS was used to further study the chemical states of C, N, and S in the products obtained by steps (1−4) (Figure 3), as indicated by the S 2p core level XPS spectra (Figure 3A). The S $2p_{3/2}$ and $2p_{1/2}$ binding energies of the first step product are centered at 163.6 and 164.6 eV, which are attributed to the C−S bond, higher than those (161.9 and 163.1 eV) of the C═S

dx.doi.org/10.1021/cs5006597 | *ACS Catal.* 2014, 4, 3302−3306

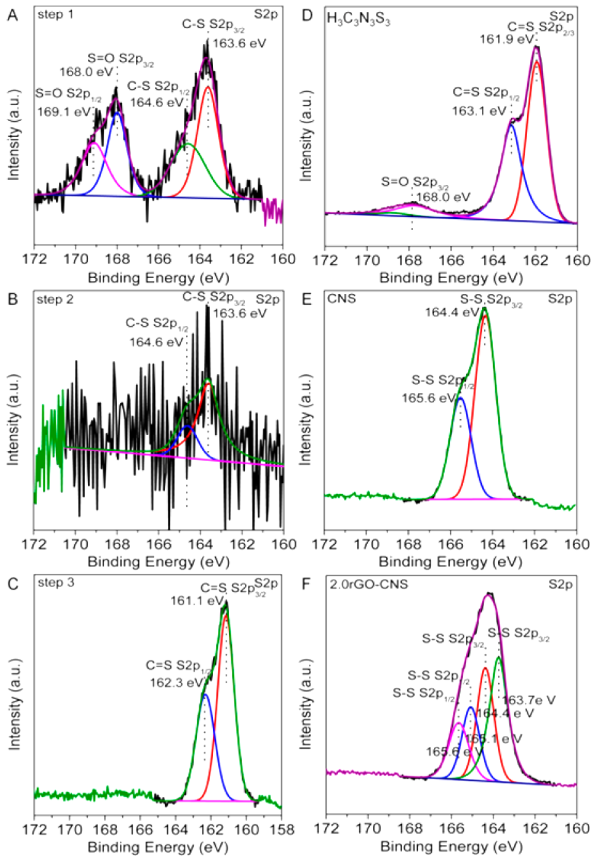

Figure 3. XPS spectra for S 2p of product of every step (A–C), $H_3C_3N_3S_3$ monomer (D), CNS (E), and 2.0rGO–CNS (F).

bonds in the $H_3C_3N_3S_3$ precursor (Figure 3D).[38] It indicates the successful pregrafting of $C_3N_3S_3$ on GO. The set of intense peaks centered at 168.0, and 169.1 eV, belonging to SO_4^{2-},[39] is a powerful evidence for the oxidation of part of the monomers by strong oxidizing groups of GO. After the chemical reduction, a very small amount of grafted $C_3N_3S_3$ species are firmly anchored on rGO, as demonstrated by the very weak S 2p lines centered at 163.6 and 164.6 eV (Figure 3B). The XPS lines of these SO_4^{2-} species disappear, showing the complete removal of those oxidized $C_3N_3S_3$. Compared to that (164.4 eV) of the $C_3N_3S_3$ polymer (Figure 3E), the S $2p_{3/2}$ binding energy of these grafted $C_3N_3S_3$ shifts by 0.8 eV toward low energy. It implies the strong electron donation of rGO to the $C_3N_3S_3$ rings as a result of the π-electron conjugated effect. The electron donation is also observed in the rGO adsorbing $C_3N_3S_3H_3$ monomers (Figure 3C). It shows the lower S $2p_{3/2}$ and $2p_{1/2}$ binding energies at 161.1 and 162.3 eV. But after adding I_2, the resultant hybrid, 2.0rGO–CNS, gives two sets of binding energies as seen clearly from the S 2p core levels (Figure 3F). The set of S 2p core levels centered at 163.7 and 165.1 eV is originated from the $C_3N_3S_3$ polymer grafted to rGO surface, whereas the set of XPS signals at 164.4 and 165.6 eV is fully consistent with that of the pure $C_3N_3S_3$ polymer. These results indicate the successful formation of the S–S bonds by the polymerization.[19]

UV–vis DRS was applied to study the optical properties of the rGO/$C_3N_3S_3$ hybrids. As shown in Supporting Information, Figure S3, the pure $C_3N_3S_3$ polymer has absorption with a band edge at 450 nm, corresponding to the band gap energy of 2.76 eV. Adding rGO, the intensity of absorption in the visible-light region is significantly improved. This is mainly because that rGO can enhance the background absorption.[30,40] Moreover, the red-shift of the absorption edge can be apparently observed for these rGO/$C_3N_3S_3$ hybrids. This clearly indicates the enhancement of solar energy utilization, as a result of the solid bond between $C_3N_3S_3$ polymers and rGO. Expectedly, the improvement of optical properties facilitates the photocatalyzed conversion of solar-to-chemical energy.

Selective aerobic oxidation of benzyl alcohol, a classic reaction, was employed to evaluate the photocatalytic properties of the rGO/$C_3N_3S_3$ hybrids. The reaction was conducted under visible light irradiation and with molecular oxygen as the primary oxidant. Figure 4A shows the photocatalytic activity of

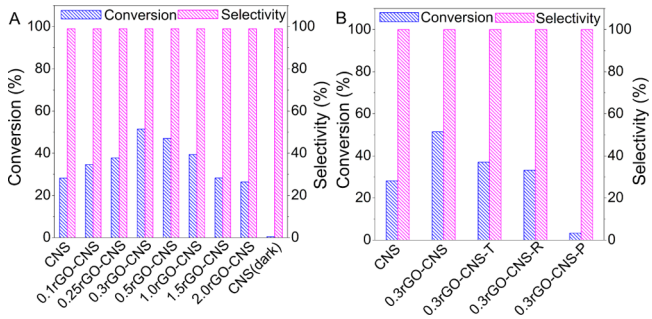

Figure 4. Photocatalytic oxidation of benzyl alcohol over pure $C_3N_3S_3$ polymer and xrGO–CNS hybrids (A) and over the 0.3rGO–CNS hybrids prepared with different methods (B).

the pure $C_3N_3S_3$ polymer and the rGO/$C_3N_3S_3$ hybrids with different rGO weight ratios. It appears that 100% selectivity implies the application potential of the polymer materials in green chemistry. Compared to the pure polymer, a distinct improvement can be observed for these rGO/$C_3N_3S_3$ hybrids. The photocatalytic conversion of benzyl alcohol increases with increasing the rGO content and reaches a maximum at 0.3 wt % of rGO, where a near double conversion up to 51.5% is achieved over the hybrid 0.3rGO–CNS. The highest light quantum yield of 2.3% is attained for the photocatalytic oxidation of benzyl alcohol under 450 nm single wavelength light irradiation. It suggests that the optimal addition of rGO is 0.3 wt %. However, a higher addition (more than 0.3 wt %) of rGO contrarily leads to a gradual decrease in the photocatalytic activity. Especially for the 2.0rGO–CNS, it shows a lower conversion than the pure $C_3N_3S_3$ polymer, indicating that the excessive rGO is deleterious to the photoreaction. Also, under solar light irradiation, the hybrid 0.3rGO–CNS achieves a conversion of 45.9% within 4 h, which is nearly 2 times than that (24.3%) of the reference anatase TiO_2 (Table 1). Moreover, use of TiO_2 is deleterious to the selectivity to benzaldehyde due to the deep-oxidation, although the 0.3rGO–CNS maintains 100% selectivity and high activity stability within 24 h. The results further confirm the application potential of the hybrid materials in chemical synthesis.

4-Nitrobenzyl alcohol, 4-methylbenzyl alcohol, and 4-fluorobenzyl alcohol were chosen to prove the wide applicability of the rGO/$C_3N_3S_3$ hybrids (Table 1). For the four reactions, 100% selectivity is achieved, but the conversion rate is related closely to the electron donation of the –R group, which decreases in the order of $-CH_3$ (54.4%) > –H (51.5%) > $-NO_2$ (34.1%) > –F (25.4%). Compared to the activity results of the pure $C_3N_3S_3$ polymer, these conversion rates are also nearly doubled over the 0.3rGO–CNS photocatalyst.

dx.doi.org/10.1021/cs5006597 | ACS Catal. 2014, 4, 3302–3306

Table 1. Photocatalytic Oxidation of Several Typical Aromatic Alcohols over the Pure $C_3N_3S_3$ Polymer (CNS) and the rGO/$C_3N_3S_3$ Hybrid (0.3rGO−CNS)[a]

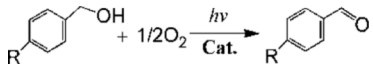

R groups	photocatalysts	conversion (%)	selectivity (%)[c]
H	CNS	28.2	100
	0.3rGO−CNS	51.5	100
NO_2[b]	CNS	22.3	100
	0.3rGO−CNS	34.1	100
F	CNS	13.5	100
	0.3rGO−CNS	25.4	100
CH_3	CNS	34.7	100
	0.3rGO−CNS	54.4	100
H[d]	0.3rGO−CNS	45.9	100
	TiO_2	24.3	92.7

[a]Reaction conditions: aromatic alcohols (0.5 mmol), photocatalysts (0.03 g), solvent of benzotrifluoride (BTF) (2.5 mL) prior to being saturated with molecular oxygen, visible light iradition (λ > 420 nm), irradiation time (8 h). [b]4-nitrobenzyl alcohol (0.05 mmol), solvent of BTF (3.5 mL). [c]The selectivity is indicated to the corresponding aldehydes. [d]The photoreaction proceeds for 4 h with sunlight irradiation.

According to the characterizations above, it is reasonable to propose that the improved photoactivity might be contributed mainly from the unique layered structure, which can ensure the intimate contact between rGO and $C_3N_3S_3$ polymers and consequently acceleration of the photogenerated electron transfer from the $C_3N_3S_3$ polymer to rGO. The decrease trend of the photocatalytic conversion upon larger than 0.3 wt % of rGO content originates from the strongly shielding effect of rGO.[13,29,30] The excessive rGO greatly shields the polymer from absorbing visible light and decreases the active sites on the surface of the polymer.

To verify the contribution of the layered "sandwich" structure to the enhanced photocatalytic conversion, we prepared three counterparts with a 0.3 wt % of rGO by varying the preparation procedure. The sample 0.3rGO−CNS-T was prepared by direct addition of the $C_3N_3S_3Na_3$ monomer into the rGO dispersion solution at the first step and without the third step, and the sample 0.3rGO−CNS-R was prepared by first reducing GO into rGO (step 2), adding the $C_3N_3S_3Na_3$ monomer (step 1), and then by adding $H_3C_3N_3S_3$ (step 3). The sample 0.3rGO−CNS-P was fabricated through ultrasonic treatment of the mixture of rGO dispersion and polymer sol. The corresponding photoactivity results were displayed in Figure 4B. The photocatalytic conversion decreases in the order of 0.3rGO−CNS (51.5%) > 0.3rGO−CNS-T (37.0%) > 0.3rGO−CNS-R (33.2%) > CNS (28.2%) > 0.3rGO−CNS-P (3.3%), indicating that the route to 0.3rGO−CNS is indeed the optimal synthesis procedure for the rGO/$C_3N_3S_3$ hybrids, which can maximize the combinative benefits from rGO and the $C_3N_3S_3$ polymer. The synthesis strategy of 0.3rGO−CNS may offer dual advantages over these preparation routes of 0.3rGO−CNS-T, -R, and -P. On the one hand, the existence of the $C_3N_3S_3Na_3$ monomer in the GO solution prior to the chemical reduction of GO is likely to prevent graphene sheets from the restacking. On the other hand, more amounts of the $C_3N_3S_3$ polymer can be anchored to rGO by the C−S bonds as demonstrated by the aforementioned XPS results. The lowest activity for the 0.3rGO−CNS-P is probably due to the drastic shielding of graphene from the light absorption of the polymer and decreases the active sites on the surface of the polymer.

Electrochemical analysis including transient photocurrent response and electrochemical impendence spectra was conducted to better understand the improvement mechanism. On the *I*−*t* curves (Figure 5A) of the pure $C_3N_3S_3$ polymer and

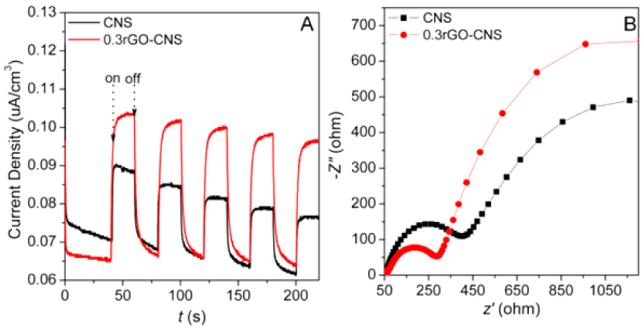

Figure 5. Photocurrent responses of the pure $C_3N_3S_3$ polymer and 0.3rGO−CNS (A). Electrochemical impedance spectroscopy (EIS) Nyquist diagrams of the pure $C_3N_3S_3$ polymer and 0.3rGO−CNS (B) in the electrolyte composed of KCl aqueous solution (0.5 M) and $K_3[Fe(CN)_6]/K_4[Fe(CN)_6]$ (0.01 M) with a ratio of 1:1.

the 0.3rGO−CNS hybrid, a near double enhancement of transient photocurrent is displayed for the 0.3rGO−CNS hybrid, compared to the pure polymer. It is in line with the activity results. This is mainly due to the superior carrier mobility of rGO. A smaller hemicycle at high frequency, which corresponds to the double-layer capacitance can be observed for the 0.3rGO−CNS electrode in the Nyquist plots (Figure 5B), further confirming the more efficient transfer of photogenerated carriers as a result of the insertion of rGO. Based on all characterizations and analysis above as well as the relative literatures,[15] we believe that the activity improvement over the rGO/$C_3N_3S_3$ hybrids follow a mechanism initiated by photogenerated electron transfer during the organic transformation (Scheme 2). With light stimulation, the HOMO

Scheme 2. Schematic Illustration of the Photocatalytic Process and the Synergetic Interaction between $C_3N_3S_3$ Polymer and rGO

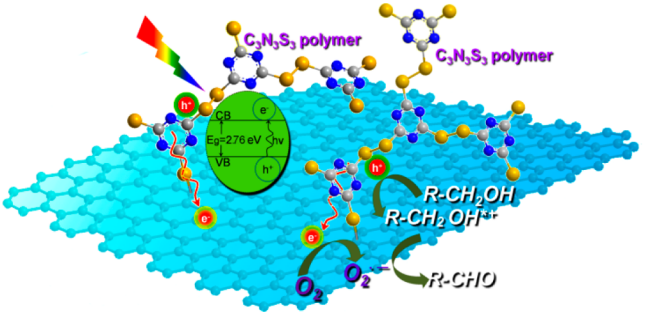

electrons of the $C_3N_3S_3$ polymer moieties jump to the LUMO orbitals and then are transferred quickly to the rGO moieties to reduce O_2 molecules, whereas the photogenerated holes oxidize the organic substrates to carbocations. The formed superoxide radicals further react with carbocations to form the final products. The layered "sandwich" structure of the rGO/$C_3N_3S_3$ hybrids can maximize the separation efficiency of photogenerated carriers of the $C_3N_3S_3$ polymer.

dx.doi.org/10.1021/cs5006597 | ACS Catal. 2014, 4, 3302−3306

In conclusion, the metal-free $C_3N_3S_3$ polymer has been found for the first time to enable selective photocatalytic oxidization of benzylic alcohols into corresponding aldehydes under visible light irradiation. More importantly, the conversion can be greatly enhanced by fabricating the layered sandwich rGO/$C_3N_3S_3$ hybrids. This study affords a novel strategy to prepare graphene-filled $C_3N_3S_3$ polymer composites for the visible light photocatalysis and demonstrates its great potential in developing metal-free $C_3N_3S_3$ polymer-based photocatalysts for the photocatalyzed synthesis of fine chemicals.

■ ASSOCIATED CONTENT

Supporting Information

Details of the hybrids fabrication and characterization including FT-IR spectra, Raman spectra, UV−vis diffuse reflectance spectra, XRD data, and the photocatalytic activity testing are provided. This material is available free of charge via the Internet at http://pubs.acs.org.

■ AUTHOR INFORMATION

Corresponding Author

*E-mail: jllong@fzu.edu.cn. Fax: +86-591-83779121. Tel.: +86-591-83779121.

Author Contributions

All authors have given approval to the final version of the manuscript.

Notes

The authors declare no competing financial interest.

■ ACKNOWLEDGMENTS

The manuscript was completed with all authors' dedication. This work was financially supported by the NSFC (Grant Nos. 21003021, 21373051, and U1305242), the Science and Technology project of the Education Office of Fujian Province of P. R. China (JA12017), and National Basic Research Program of China (973 Program, No. 2012CB722607).

■ REFERENCES

(1) Pina, C. D.; Falletta, E.; Rossi, M. *J. Catal.* **2008**, *260*, 384−386.
(2) Dess, D. B.; Martin, J. C. *J. Am. Chem. Soc.* **1991**, *113*, 7277−7287.
(3) Long, J.; Xie, X.; Xu, J.; Gu, Q.; Chen, L.; Wang, X. *ACS Catal.* **2012**, *2*, 622−631.
(4) Gamez, P.; Arends, I. W. C. E.; Reedijk, J.; Sheldon, R. A. *Chem. Commun.* **2003**, 2414−2415.
(5) Mori, K.; Hara, T.; Mizugaki, T.; Ebitani, K.; Kaneda, K. *J. Am. Chem. Soc.* **2004**, *126*, 10657−10666.
(6) Abad, A.; Concepción, P.; Corma, A.; García, H. *Angew. Chem., Int. Ed.* **2005**, *44*, 4066−4069.
(7) Zhao, M.; Li, J.; Mano, E.; Song, Z.; Tschaen, D. M.; Grabowski, E. J. J.; Reider, P. J. *J. Org. Chem.* **1999**, *64*, 2564−2566.
(8) Besson, M.; Gallezot, P. *Catal. Today* **2000**, *57*, 127−141.
(9) Palmisano, G.; García-López, E.; Marcì, G.; Loddo, V.; Yurdakal, S.; Augugliaro, V.; Palmisano, L. *Chem. Commun.* **2010**, *46*, 7074−7089.
(10) Fukuzumi, S.; Kuroda, S.; Tanaka, T. *J. Am. Chem. Soc.* **1985**, *107*, 3020−3027.
(11) Yurdakal, S.; Palmisano, G.; Loddo, V.; Augugliaro, V.; Palmisano, L. *J. Am. Chem. Soc.* **2008**, *130*, 1568−1569.
(12) Chao, D.; Fu, W. F. *Dalton Trans.* **2014**, *43*, 306−310.
(13) Zhang, N.; Zhang, Y.; Pan, X.; Fu, X.; Liu, S.; Xu, Y. *J. Phys. Chem. C* **2011**, *115*, 23501−23511.
(14) Tanaka, A.; Hashimoto, K.; Kominami, H. *Chem. Commun.* **2011**, *47*, 10446−10448.
(15) Su, F.; Mathew, S. C.; Lipner, G.; Fu, X.; Antonietti, M.; Blechert, S.; Wang, X. *J. Am. Chem. Soc.* **2010**, *132*, 16299−16301.
(16) Long, J.; Wang, S.; Ding, Z.; Wang, S.; Zhou, Y.; Huang, L.; Wang, X. *Chem. Commun.* **2012**, *48*, 11656−11658.
(17) Zhang, M.; Chen, C.; Ma, W.; Zhao, J. *Angew. Chem., Int. Ed.* **2008**, *120*, 9876−9879.
(18) Chen, Z.; Xu, J.; Ren, Z.; He, Y.; Xiao, G. *J. Solid State Chem.* **2013**, *205*, 134−141.
(19) Zhang, Z.; Long, J.; Yang, L.; Chen, W.; Dai, W.; Fu, X.; Wang, X. *Chem. Sci.* **2011**, *2*, 1826−1830.
(20) Cai, D.; Song, M. *J. Mater. Chem.* **2010**, *20*, 7906−7915.
(21) Novoselov, K. S. *Angew. Chem., Int. Ed.* **2011**, *50*, 2−19.
(22) Zhao, G.; Li, J.; Jiang, L.; Dong, H.; Wang, X.; Hu, W. *Chem. Sci.* **2012**, *3*, 433−437.
(23) Wang, S.; Goh, B. M.; Manga, K. K.; Bao, Q.; Yang, P.; Loh, K. P. *ACS Nano* **2010**, *4*, 6180−6186.
(24) Wang, X.; Song, M. *Nanomater. Energy* **2013**, *2*, 265−278.
(25) Rafiq, R.; Cai, D.; Jin, J.; Song, M. *Carbon* **2010**, *48*, 4309−4314.
(26) Zhang, H.; Lv, X.; Li, Y.; Wang, Y.; Li, J. *ACS Nano* **2010**, *4*, 380−386.
(27) Xiang, Q.; Yu, J.; Jaroniec, M. *J. Phys. Chem. C* **2011**, *115*, 7355−7363.
(28) Lightcap, L. V.; Kosel, T. H.; Kamat, P. V. *Nano Lett.* **2010**, *10*, 577−583.
(29) Zhang, Y.; Tang, Z.-R.; Fu, X.; Xu, Y.-J. *ACS Nano* **2010**, *4*, 7303−7314.
(30) Yu, J.; Jin, J.; Cheng, B.; Jaroniec, M. *J. Mater. Chem. A* **2014**, *2*, 3407−3416.
(31) Verdejo, R.; Bernal, M. M.; Romasanta, L. J.; Lopez-Manchado, M. A. *J. Mater. Chem.* **2011**, *21*, 3301−3310.
(32) Kim, H.; Abdala, A. A.; Macosko, C. W. *Macromolecules* **2010**, *43*, 6515−6530.
(33) Li, D.; Müller, M. B.; Gilje, S.; Kaner, R. B.; Wallace, G. G. *Nat. Nanotechnol.* **2008**, *3*, 101−105.
(34) Leofanti, G.; Padovan, M.; Tozzola, G.; Venturelli, B. *Catal. Today* **1998**, *41*, 207−219.
(35) Zhang, N.; Liu, S.; Fu, X.; Xu, Y. *J. Phys. Chem. C* **2011**, *115*, 22901−22909.
(36) Loughran, G. A.; Ehlers, G. F. L.; Crawford, W. J.; Burkett, J. L.; Ray, J. D. *Appl. Spectrosc.* **1964**, *18*, 129−134.
(37) Mieczys, A.; Kucharski, E. C. *J. Appl. Polym. Sci.* **2000**, *76*, 439−445.
(38) Mori, K.; Suzuki, K.; Shimizu, K.; Oishi, Y. *Langmuir* **2002**, *18*, 9527−9532.
(39) Ishida, T.; Fukushima, H.; Mizutani, W.; Miyashita, S.; Ogiso, H.; Ozaki, K.; Tokumoto, H. *Langmuir* **2002**, *18*, 83−92.
(40) Li, Q.; Guo, B.; Yu, J.; Ran, J.; Zhang, B.; Yan, H.; Gong, J. *J. Am. Chem. Soc.* **2011**, *133*, 10878−10884.